Theoretical Study of the Interactions between Cations and Anions in Group IV Transition-Metal Catalysts for Single-Site Homogeneous Olefin Polymerization

Zhitao Xu, Kumar Vanka, Timothy Firman, Artur Michalak, Eva Zurek, Chuanbao Zhu, and Tom Ziegler*

Department of Chemistry, University of Calgary, Calgary, Alberta, Canada T2N 1N4

Received December 14, 2001

Density functional theory has been used to investigate the interaction between a series of cationic polymerization catalysts and their anionic counterions. The catalyst systems include $(NPR_3)_2TiMe^+$, $(Cp)(NCR_2)TiMe^+$, $(CpSiR_2NR')TiMe^+$, $(Cp)OSiR_3TiMe^+$, and $(Cp)NPR_3TiMe^+$. The counterions studied are $B(C_6F_5)_4^-$, $MeB(C_6F_5)_3^-$, TMA-MAOMe$^-$, and MAOMe$^-$, where TMA = trimethylaluminum and MAO = methylalumoxane. Two simplified model structures, which have been proposed as the counterions for the active (TMA-MAOMe$^-$) and dormant (MAOMe$^-$) ion pairs in single-site catalysts activated by MAO, were used for the last two counterions. The interaction between the cation and anion will be discussed in terms of ion-pair formation and separation energies. Full quantum-mechanical (QM) calculations demonstrate that, for the same catalyst system but different anions, the ion-pair separation energies increase in the order $B(C_6F_5)_4^- < MeB(C_6F_5)_3^-$ < TMA-MAOMe$^-$ < MAOMe$^-$. For the same counterion but different cations, the $(NPR_3)_2TiMe^+$ system has the lowest separation energy. Increasing the size of the R group decreases the ion-pair separation energy. Combined quantum-mechanical (QM) and molecular-mechanical (MM) models (QM/MM) for $MeB(C_6F_5)_3^-$ and TMA-MAOMe$^-$ have also been developed and examined by comparing the ion-pair formation and separation energies to the full QM results. The QM parts of $MeB(C_6F_5)_3^-$ and TMA-MAOMe$^-$ are represented by $MeBCl_3^-$ and $MeBMe_2Cl^-$, respectively. The other parts of the anions are replaced by MM atoms. Preliminary studies on olefin insertion reactions for the $(NPH_3)_2TiMe-\mu Me-A$ (A = $B(C_6F_5)_3$ and TMA-MAO) systems suggest that the QM/MM models satisfactorily reproduce the behavior of the ion-pair system in the insertion process.

Introduction

Single-site homogeneous catalysts have in recent years received increasing attention as alternatives to traditional Ziegler−Natta type heterogeneous catalysts. This is primarily due to their ability to achieve good stereoselectivity, a narrow molecular weight distribution, and high activity.[1] Another advantage is that these systems are structurally well defined mononuclear species. Systematic modification of their structures thus allows for enhanced control over polymer properties. Among the more highly active homogeneous catalysts are metallocenes and related organometallic compounds containing a group 4 transition metal.

Single-site olefin polymerization precatalysts often contain a group 4 transition-metal center (M) coordinated to two ligands (L, L′) and two alkyl groups (R, R′): LL′MRR′. Such neutral complexes by themselves are not effective as polymerization catalysts but require activation by a cocatalyst. The cocatalysts are generally Lewis acids, such as tris(pentafluorophenyl)borane or methylalumoxane (MAO), whose function is to abstract one of the alkyl groups as R$^-$ to produce the activated cationic catalyst LL′MR′$^+$.[2] The accepted mechanism for the uptake and insertion of the olefin monomer into the metal−carbon bond in the cationic catalyst is shown in Figure 1 with ethylene as the olefin monomer.

If the counterions are ignored, the well-defined molecular structures of the single-site catalysts allow for thorough mechanistic studies by theoretical methods, and several theoretical studies have been conducted.[3]

(1) For recent reviews, see: (a) Coates, G. W. *Chem. Rev.* **2000**, *100*, 1223. (b) Chen, E. Y. X.; Marks, T. J. *Chem. Rev.* **2000**, *100*, 1391. (c) Rappé, K.; Skiff, W. M.; Casewit, C. J. *Chem. Rev.* **2000**, *100*, 1435.

(2) (a) Bochmann, M. *J. Chem. Soc., Dalton Trans.* **1996**, 225. (b) Pasynkiewicz, S. *Polyhedron* **1990**, *9*, 429. (c) Mason, M. R.; Smith, J. M.; Bott, S. G.; Barron, A. R. *J. Am. Chem. Soc.* **1993**, *115*, 4971. (d) Atwood, J. L.; Hrncir, D. C.; Priester, R. D.; Rogers, R. D. *Organometallics* **1983**, *2*, 985. (e) Harlan, C. J.; Bott, S. G.; Barron, A. R. *J. Am. Chem. Soc.* **1995**, *117*, 6465. (f) Barron, A. R. 218th National Meeting of the American Chemical Society, New Orleans, LA, August 22−26, 1999. (g) Yang, X.; Stern, C. L.; Marks, T. J. *J. Am. Chem. Soc.* **1994**, *116*, 10015. (h) Deck, P. A.; Marks, T. J. *J. Am. Chem. Soc.* **1995**, *117*, 6128. (i) Jia, L.; Stern, C. L.; Marks, T. J. *Organometallics* **1997**, *16*, 842. (j) Li, L.; Marks, T. J. *Organometallics* **1998**, *17*, 3996. (k) Deck, P.; Beswick, C. L.; Marks, T. J. *J. Am. Chem. Soc.* **1998**, *120*, 1772.

(3) (a) Woo, T. K.; Margl, P. M.; Ziegler, T.; Blöchl, P. E. *Organometallics* **1997**, *16*, 3454. (b) Woo, T. K.; Margl, P. M.; Lohrenz, J. C. W.; Blöchl, P. E.; Ziegler, T. *J. Am. Chem. Soc.* **1996**, *118*, 13021. (c) Margl, P. M.; Lohrenz, J. C. W.; Ziegler, T.; Blöchl, P. E. *J. Am. Chem. Soc.* **1996**, *118*, 4434. (d) Fan, L.; Harrison, D.; Woo, T. K.; Ziegler, T. *Organometallics* **1995**, *14*, 2018. (e) Meier, R. J.; Doremaele, G. H. J. V.; Tarlori, S.; Buda, F. *J. Am. Chem. Soc.* **1994**, *116*, 7274. (f) Yoshida, T.; Koga, N.; Morokuma, K. *Organometallics* **1995**, *14*, 746. (g) Weiss, H.; Ehrig, M.; Ahlrichs, R. *J. Am. Chem. Soc.* **1994**, *116*, 4919. (h) Bierwagen, E. P.; Bercaw, J. E.; Goddard, W. A. III. *J. Am. Chem. Soc.* **1994**, *116*, 1481.

10.1021/om011057c CCC: $22.00
Publication on Web 05/16/2002

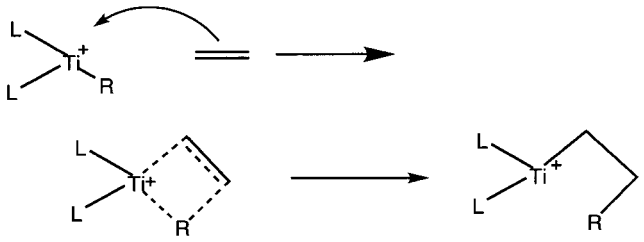

Figure 1. Reaction mechanism for uptake and insertion of olefin into the metal−carbon bond of the cation.

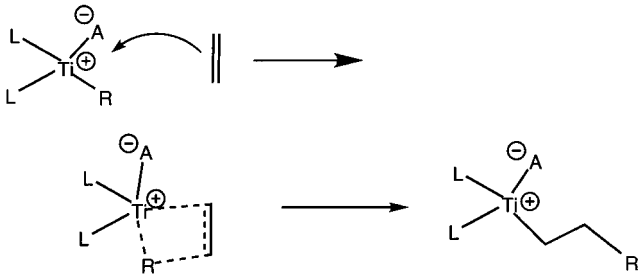

Figure 2. Reaction mechanism for uptake and insertion of olefin into the metal−carbon bond of the ion-pair.

However, recent experimental[2g−j,4] and theoretical[5,6] results show that the anionic counterions play an important role in the polymerization process (Figure 2). Anionic counterions that will be investigated here are shown in Figure 3. They include $MeB(C_6F_5)_3^-$ (Me = CH_3), $B(C_6F_5)_4^-$, TMA-MAOMe$^-$ (TMA = trimethylaluminum), and MAOMe$^-$. The last two have been proposed as simplified models for the counterions in the active (TMA-MAOMe$^-$) and dormant (MAOMe$^-$) ion pairs of single-site catalysts activated by MAO, although the real structures of MAO are not yet fully understood.[7]

In the present study, density functional theory has been used to investigate the interaction between a series of cationic catalysts and their anionic counterions. The cationic catalyst systems studied include $(NPR_3)_2TiMe^+$,[8] $(Cp)(NCR_2)TiMe^+$,[9] $(CpSiR_2NR')TiMe^+$,[10] $(Cp)OSiR_3TiMe^+$, and $(Cp)NPR_3TiMe^+$.[11] $(1,2\text{-}Me_2Cp)_2ZrMe^+$,[1b] which has been known as a good catalyst, has also been studied for the purpose of comparison. Figure 4 displays the structures of these cationic catalyst systems.

The interaction between the cation and anion will be discussed in terms of ion-pair formation and separation energies. We calculated the ion-pair formation energies based on

$$LL'MMe_2 + A \rightarrow [LL'MMe]^+[MeA]^- + \Delta H_{ipf} \quad (1)$$

where L, L′ = Cp, NPR_3, NCR_2, $OSiR_3$, $CpSi(Me)_2NR$, A = $B(C_6F_5)_3$, MAO, TMA-MAO, and ΔH_{ipf} = enthalpy of ion-pair formation.

On the other hand, separation energies are calculated according to

$$[LL'MMe]^+[MeA]^- \rightarrow [LL'MMe]^+ + MeA^- + \Delta H_{ips} \quad (2)$$

where ΔH_{ipf} = enthalpy of ion-pair separation and A = $B(C_6F_5)_3$, MAO, TMA-MAO.

For the anion $B(C_6F_5)_4^-$, we calculate the separation energy ΔH_{ips} according to

$$LL'MMe{-}B(C_6F_5)_4 \rightarrow LL'MMe^+ + B(C_6F_5)_4^- + \Delta H_{ips} \quad (3)$$

This first part should provide a systematic understanding of how electronic and steric factors influence the stability of the ion pairs. The results obtained here will be compared to data from similar calculations carried out on different systems in previous, more limited studies.[6g,h]

The considerable size of the counterions makes studies of monomer insertion into the metal−carbon bond in the presence of the counterion costly and time-consuming. Therefore, modeling the counterion using combined quantum-mechanical and molecular-mechanical (QM/MM)[12] methods is an attractive alternative. We shall propose here QM/MM models for $B(C_6F_5)_3Me^-$ and TMA-MAOMe$^-$. The ion-pair formation and dissociation energies calculated by using these QM/MM models will be compared to those from full QM calculations with and without solvent effects included. Thus, the second part of the study should provide good QM/MM models of the anions for future polymerization studies.

Computational Details

Density functional theory (DFT) calculations were carried out on the basis of the Amsterdam Density Functional (ADF) program, version 2000.01, developed by Baerends et al.[13] and vectorized by Ravenek.[14] The numerical integration scheme applied was developed by te Velde et al.,[15] and the geometry optimization procedure was based on the method of Verslius

(4) (a) Siedle, A. R.; Newmark, R. A.; Lamanna, W. M.; Shroepfer, J. N. *Polyhedron* **1990**, *9*, 301. (b) Bochmann, M.; Lancaster, S. J. *Angew. Chem., Int. Ed. Engl.* **1994**, *33*, 1634. (c) Bochmann, M.; Lancaster, S. J. *J. Organomet. Chem.* **1995**, *497*, 55. (d) Hlatky, G. G.; Eckman, R. R.; Turner, H. W. *Organometallics* **1992**, *11*, 1413. (e) Jia, L.; Yang, X.; Stern, C. L.; Marks, T. J. *Organometallics* **1994**, *13*, 3755. (f) Chen, Y.-X.; Stern, C. L.; Marks, T. J. *J. Am. Chem. Soc.* **1997**, *119*, 2582. (g) Williams, V. C.; Piers, W. E.; Clegg, W.; Collins, S.; Marder, T. B. *J. Am. Chem. Soc.* **1999**, *121*, 3244. (h) Jelinek, T.; Baldwin, P.; Scheidt, W. R.; Reed, C. A. *Inorg. Chem.* **1993**, *32*, 1982. (i) Strauss, S. H. 218th National Meeting of the American Chemical Society, New Orleans, LA, August 22−26, 1999. (j) Chien, J. C. W.; Tsai, W. M.; Rausch, M. D. *J. Am. Chem. Soc.* **1991**, 113, 8570. (k) Giardello, M. A.; Disen, M. S.; Stern, C. L.; Marks, T. J. *J. Am. Chem. Soc.* **1995**, *117*, 12114. (l) Tritto, I.; Donetti, R.; Sacchi, M. C.; Locatelli, P.; Zannoni, G. *Macromolecules* **1999**, *32*, 264. (m) Tritto, I.; Donetti, R.; Sacchi, M. C.; Locatelli, P.; Zannoni, G. *Macromolecules* **1997**, *30*, 1247. (n) Rappe, A. K.; Skiff, W. M.; Casewit, C. J. *Chem. Rev.* **2000**, *100*, 1435 and references therein.

(5) Chan, M. S. W.; Ziegler, T. *Organometallics* **2000**, 19, 5182.

(6) (a) Lanza, G.; Fragala, I. L.; Marks, T. J. *J. Am. Chem. Soc.* **1998**, *120*, 8257. (b) Lanza, G.; Fragala, I. L. *Top. Catal.* **1999**, *7*, 45. (c) Klesing, A.; Bettonville, S. *Phys. Chem. Chem. Phys.* **1999**, *1*, 2373. (d) Fusco, R.; Longo, L.; Masi, F.; Garbassi, F. *Macromol. Rapid Commun.* **1998**, *19*, 257. (e) Fusco, R.; Longo, L.; Masi, F.; Garbassi, F. *Macromolecules* **1997**, *30*, 7673. (f) Bernardi, F.; Bottoni, A.; Miscione, G. P. *Organometallics* **1998**, *17*, 16. (g) Chan, M. S. W.; Vanka, K.; Pye, C. C.; Ziegler, T. *Organometallics* **1999**, *18*, 4624. (h) Vanka, K.; Chan, M. S. W.; Pye, C. C.; Ziegler, T. *Organometallics* **2000**, *19*, 1841. (i) Vanka, K.; Ziegler, T. *Organometallics* **2001**, 20, 905.

(7) (a) Zurek, E.; Ziegler, T.; *Organometallics* **2002**, *21*, 83−92. (b) Zakharov, I. I.; Zakharov, V. A. *Macromol. Theory Simul.* **2001**, *10*, 108.

(8) Stephan, D. W.; Guérin, F.; Spence, R. E. v. H.; Koch, L.; Gao, X.; Brown, S. J.; Swabey, J. W.; Wang, Q.; Xu, W.; Zoricak, P.; Harrison, D. G. *Organometallics* **1999**, *18*, 2046.

(9) Zhang, S.; Piers, W. E.; Gao, X.; Parvez, M. *J. Am. Chem. Soc.* **2000**, *122*, 5499.

(10) Chen, Y. X.; Marks, T. J. *Organometallics* **1997**, *16*, 3649.

(11) Stephan, D. W.; Stewart, J. C.; Guérin, F.; Spence, R. E. v. H.; Xu, W.; Harrison, D. G. *Organometallics* **1999**, *18*, 1116.

(12) (a) Woo. T. K.; Cavallo, L.; Ziegler, T. *Theor. Chim. Acta* **1998**, *100*, 307. (b) Maseras, F.; Morokuma, K. *J. Comput. Chem.* **1995**, *16*, 1170.

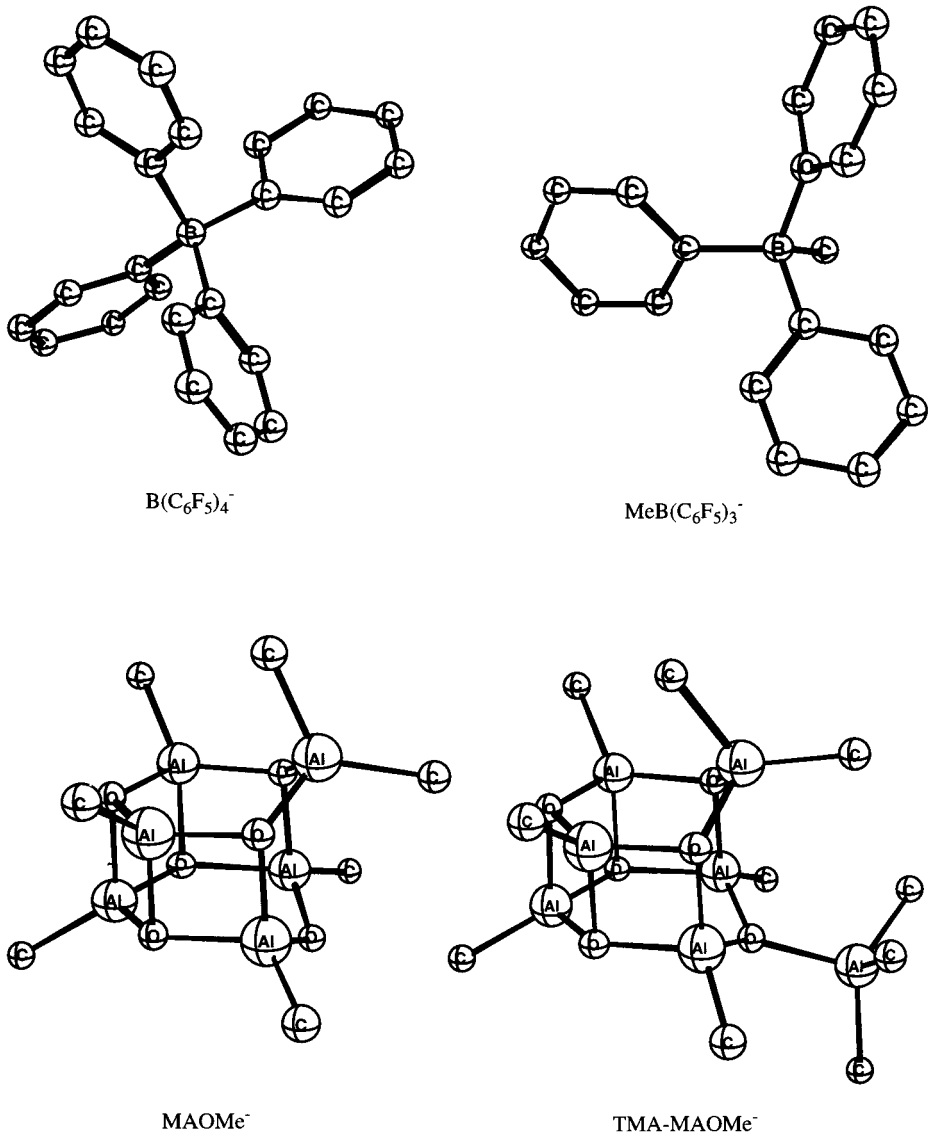

Figure 3. Structures of counterions (the H and F atoms have been omitted for the purpose of clarity).

and Ziegler.[16] Geometry optimizations were carried out using the local exchange-correlation potential of Vosko et al.[17] without any symmetry constraints. The electronic configurations of the atoms were described by a triple-ζ basis set on titanium ($n = 3$) and zirconium ($n = 4$) for *n*s, *n*p, *n*d, and ($n + 1$)s, augmented with a single ($n + 1$)p polarization function. Double-ζ STO basis sets were used for carbon (2s, 2p), hydrogen (1s), and nitrogen (2s, 2p), augmented with a single 3d polarization function, except for hydrogen, where a 2p polarization function was used. Shells of lower energy were treated by the frozen-core approximation. A set of auxiliary s, p, d, f, and g STO functions centered on all nuclei was used to fit the molecular density and represent Coulomb and exchange potentials accurately in each SCF cycle.[18] The gas-phase energy differences were calculated by augmenting the local density approximation energy with Perdew and Wang's nonlocal correlation correction and Becke's exchange corrections (PWB91).[19] The solvation energies based on gas-phase geometries were calculated by the conductor-like screening model (COSMO)[20] with a dielectric constant of 2.023 to represent cyclohexane as the solvent. The radii used for the atoms (in Å) were as follows: C, 2.0; H, 1.16; B, 1.15; N, 1.5; O, 1.5; F, 1.2; Zr, 2.4; Ti, 2.3; P, 1.7; Cl, 2.1; Si, 2.2; Al, 2.3. The enthalpies (ΔH) reported in the following sections are potential energy differences without zero point or vibrational finite temperature corrections. These terms are still too expensive to calculate for the size of molecules considered here. We expect these corrections to be on the order of $\pm 2-3$ kcal/mol. The charge distribution was analyzed by the Hirshfeld method.[21] In the calculation of the charges of ligands, each ligand (negatively charged) was considered as a fragment. Single-point calculations were carried out for the ligands using the geometries taken directly from the whole molecules. The whole molecules

(13) (a) Baerends, E. J.; Ellis, D. E.; Ros, P. *Chem. Phys.* **1973**, *2*, 41. (b) Baerends, E. J.; Ros, P. *Chem. Phys.* **1973**, *2*, 52. (c) te Velde, G.; Baerends, E. J. *J. Comput. Phys.* **1992**, *92*, 84. (d) Fonseca, C. G.; Visser, O.; Snijders, J. G.; te Velde, G.; Baerends, E. J. In *Methods and Techniques in Computational Chemistry, METECC-95*; Clementi, E., Corongiu, G., Eds.; STEF; Cagliari, Italy, 1995; p 305.

(14) Ravenek, W. In *Algorithms and Applications on Vector and Parallel Computers*; te Riele, H. J. J., Dekker: T. J., vand de Horst, H. A., Eds.; Elservier: Amsterdam, 1987.

(15) (a) te Velde, G.; Baerends, E. J. *J. Comput. Chem.* **1992**, *99*, *84*. (b) Boerrigter, P. M.; te Velde, G.; Baerends, E. J. *Int. J. Quantum Chem.* **1998**, *33*, 87.

(16) Verslius, L.; Ziegler, T. *J. Chem. Phys.* **1988**, *88*, 322.

(17) Vosko, S. H.; Wilk, L.; Nusair, M. *Can. J. Phys.* **1980**, *58*, 1200.

(18) Krijn, J.; Baerends, E. J. *Fit Functions in the HFS-Method*; Free University of Amsterdam: Amsterdam, 1984.

(19) Perdew, J. P. *Phys. Rev. B* **1992**, *46*, 6671.

(20) (a) Klamt, A.; Schuurmann, G. *J. Chem. Soc., Perkin Trans.* **1993**, *2*, 799. (b) Pye, C. C.; Ziegler, T. *Theor. Chem. Acta* **1999** V 101, 396.

(21) (a) Hirshfeld, F. L. *Theor. Chem. Acta* **1977**, *44*, 129. (b) Wiberg, K. B.; Rablen, P. R. *J. Comput. Chem.* **1993**, *1412*, 1504.

Table 1. Full QM Ion-Pair Separation Energies (ΔH_{ips},[a] kcal/mol) for Different Systems

	$B(C_6F_5)_4^-$		$B(C_6F_5)_3Me^-$		TMA-MAOMe$^-$		MAOMe$^-$	
catalyst	gas phase	soln[b]	gas phase	soln[b]	gas phase	soln[b]	gas phase	soln[b]
$(1,2\text{-}Me_2Cp)_2ZrMe^+$	55.72	23.40	86.98	52.34	87.95	51.82	104.92	63.98
$(NPMe_3)_2TiMe^+$	58.74	28.91	73.05	41.59	82.50	49.87	102.05	62.05
$(Cp)(NPMe_3)TiMe^+$	69.86	37.31	84.17	50.86	93.10	55.34	113.91	73.41
$(Cp)(NCMe_2)TiMe^+$	78.16	43.17	90.08	54.87	99.41	60.20	122.94	80.41
$(CpSiMe_2NMe)TiMe^+$	73.73	41.54	91.50	56.52	104.32	67.36	129.81	88.24
$(Cp)(OSiMe_3)TiMe^+$	76.84	42.83	91.49	55.46	102.45	64.18	122.02	79.20

[a] Corresponding to the process $[LL'MMe]^+[A]^- \rightarrow [LL'MMe]^+ + A^- + \Delta H_{ips}$, where A = $MeB(C_6F_5)_3^-$, $B(C_6F_5)_4^-$, MAOMe$^-$, TMA-MAOMe$^-$. [b] Solvent: cyclohexane ($\epsilon = 2.023$).

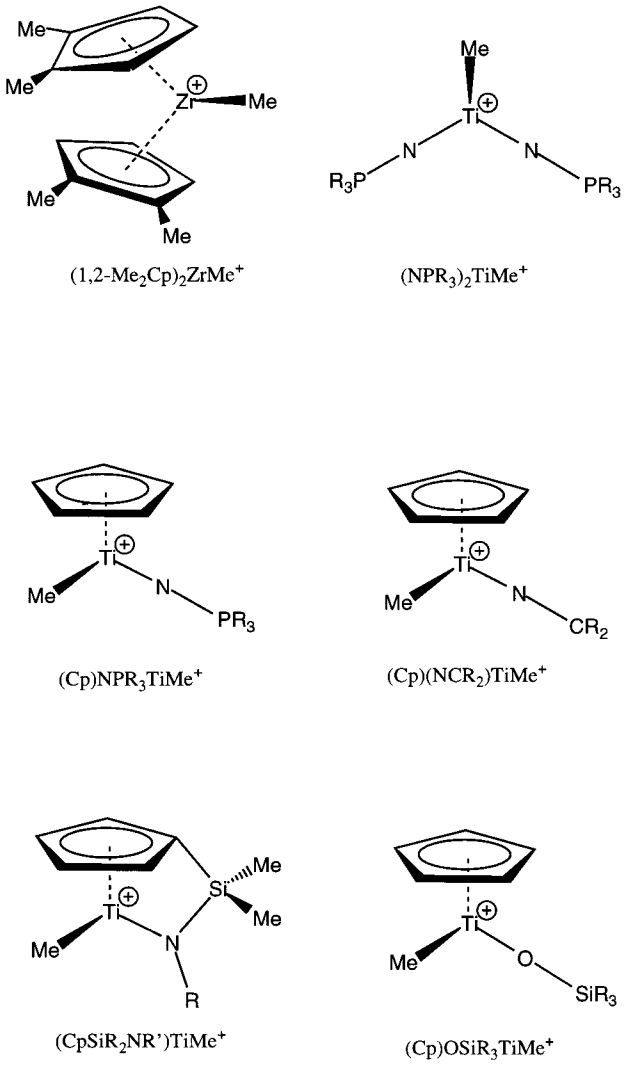

Figure 4. Structures of different catalyst systems.

were then calculated using the results of ligands as fragments. The insertion barriers were obtained from linear transit calculations with the C−C distance between one C of the ethylene and the carbon of the Me group, which represents the growing chain, as reaction coordinate. In our QM/MM modeling, the QM part of $B(C_6F_5)_3Me^-$ is represented by $MeBCl_3^-$ and $MeAlClMe_2^-$ is used to describe the QM part of TMA-MAOMe$^-$. The remaining parts (see Figure 5) are described by molecular mechanics (MM) using the SYBYL/TRIPOS 5.2 force field constants,[22] without electrostatic interactions. Solvent effects were taken into account by single-point calculations. For our QM/MM modeling, only the QM atoms were included in solvation calculations, since the inclusion of MM atoms in solvation calculations has not yet been incorporated into ADF. The code for QM/MM in ADF has been implemented by Woo et al.[12]

(22) Clark, M.; Cramer, R. D. I.; van Opdenbosch, N. *J. Comput. Chem.* **1989**, *10*, 982.

Results and Discussions

In olefin polymerization, monomer uptake and insertion are crucial steps for the propagation of a polymer chain. Both steps are likely to be influenced by the mobility and coordination strength of the counterions, as an anion bound too strongly is unable to provide space and suitable acceptor orbitals for the incoming olefin. We present here a study of the energy required to separate an ion pair into its anionic and cationic components according to eqs 2 and 3. The ion-pair separation energy (ΔH_{ips}) can be considered as a measure for the mobility of the anion. Thus, a study of the factors shaping ΔH_{ips} provides a first important step toward an understanding of how the anion influences monomer uptake and insertion.

Ion-Pair Separation Energy (Full QM). Table 1 displays the ion-pair separation energies (ΔH_{ips}) from full QM calculations on several different titanium-based catalyst systems, i.e. $(NPR_3)_2TiMe^+$, $(Cp)NCR_2TiMe^+$, $CpNSiR_3TiMe^+$, $(Cp)OSiR_3TiMe^+$, and $(Cp)NPR_3TiMe^+$ (R = Me), associated with four different anions, $MeB(C_6F_5)_3^-$, $B(C_6F_5)_4^-$, MAOMe$^-$, and TMA-MAOMe$^-$. Data for the $(1,2\text{-}Me_2Cp)_2ZrMe^+$ system are also listed for the purpose of comparison. For the same catalyst, ion pairs of $B(C_6F_5)_4^-$ have the lowest separation energy and thus the weakest interactions between the anion and the cations. The interaction in this case is between the metal center and one or two fluorine atoms on the anion (Chart 1). In the gas phase ΔH_{ips} = 56−77 kcal/mol, whereas the corresponding values in cyclohexane are 23−43 kcal/mol (Table 1). Separation energies involving $B(C_6F_5)_4^-$ exhibit the largest energy range for the four anions. The two types of methyl-bridged ion pairs containing $MeB(C_6F_5)_3^-$ and TMA-MAOMe$^-$, respectively, have much higher separation energies (Chart 1 and Table 1). For $MeB(C_6F_5)_3^-$ the gas and solvent (cyclohexane) phase values are 87−92 and 52−56 kcal/mol, respectively. The corresponding energies for TMA-MAOMe$^-$ are 1−12 kcal/mol (gas phase) and 0−11 kcal/mol (cyclohexane) higher. The highest separation energies are calculated for ion pairs with MAOMe$^-$, where the cations and the anion are connected by a metal−oxygen bond (Chart 1). The strong metal−oxygen bonding interaction is responsible for the large ΔH_{ips} values of 105−122 kcal/mol (gas phase) and 64−88 kcal/mol (cyclohexane).

It is remarkable that ΔH_{ips} values for $B(C_6F_5)_4^-$, $MeB(C_6F_5)_3^-$, TMA-MAOMe, and MAOMe$^-$ follow the same order with respect to the cations (Table 1) except

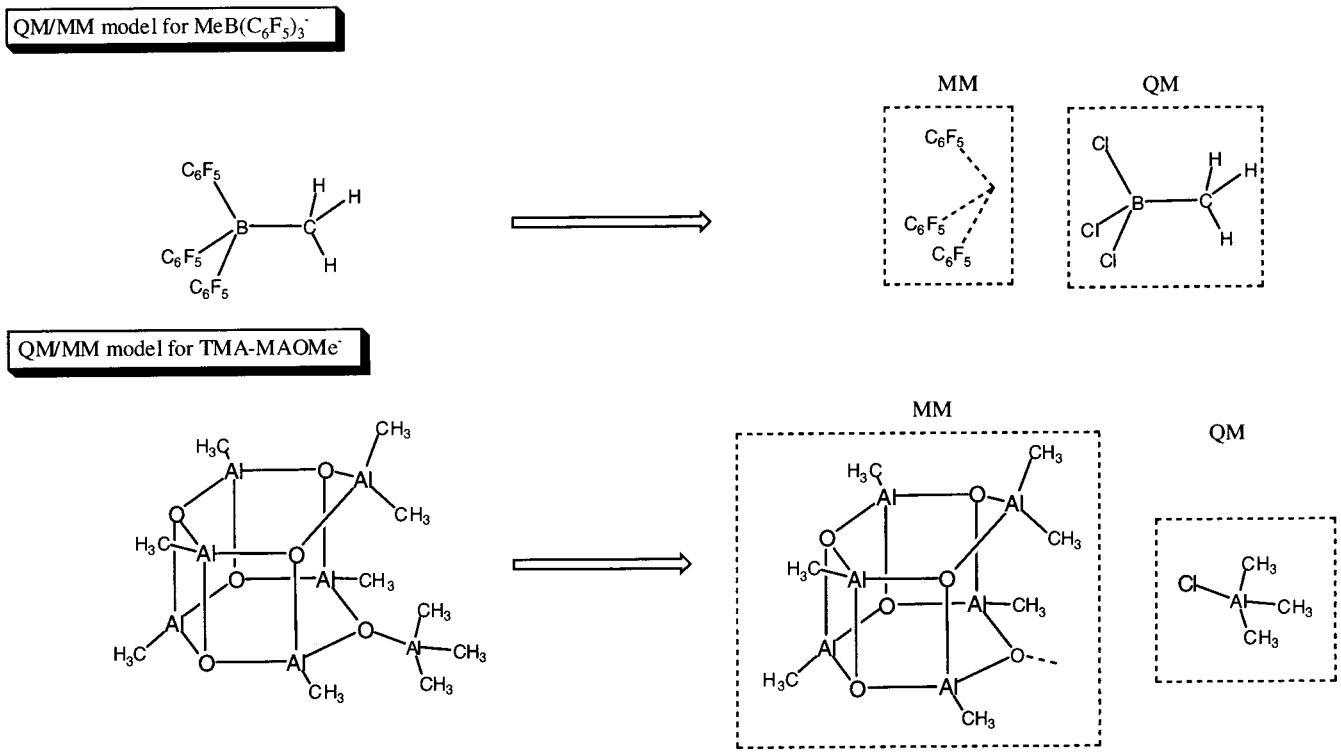

Figure 5. QM/MM models for $Me(C_6F_5)_3^-$ and TMA-MAOMe$^-$.

for ion pairs, where ΔH_{ips} values differ by a few kilocalories per mole. The order clearly reflects the different degrees to which the ancillary ligands L and L′ are able to stabilize the electron-poor metal center as the cationic species LL′MMe$^+$ emerge after the ion-pair separation.

For different cationic catalysts with the same anionic counterion, the separation energy for the $(NPMe_3)_2TiMe^+$ system is the lowest, even lower than that for $(1,2\text{-}Me_2Cp)_2ZrMe^+$. Substituting one of the two $NPMe_3$ ligands with a Cp group, forming $(Cp)(NPMe_3)TiMe^+$, increases the ion-pair separation energies by more than 10 kcal/mol in the gas phase. Replacing $NPMe_3$ in $(Cp)(NPMe_3)TiMe^+$ with another ligand, to form the $(Cp)(OSiMe_3)TiMe^+$, $(Cp)(NCMe_2)TiMe^+$, and $(CpSiMe_2NMe)TiMe^+$ systems, further increases the separation energies considerably (Table 1). Overall, the $NPMe_3$ ligand offers the lowest ion-pair separation energy compared to Cp, $OSiMe_3$, $NCMe_2$, and $CpSiMe_2NMe$ ligands. The trend does not change when solvent effects are taken into account and follows the order (except for $[(Cp)(NCMe_2)TiMe]^+[B(C_6F_5)_4]^-$)

$$Me_2Cp_2ZrMe^+ < (NPMe_3)_2TiMe^+ < (Cp)(NPMe_3)TiMe^+ < (Cp)(NCMe_2)TiMe^+ < \{(CpSiMe_2NMe)TiMe^+, (Cp)(OSiMe_3)TiMe^+\} \quad (4)$$

where $\{(CpSiMe_2NMe)TiMe^+, (Cp)(OSiMe_3)TiMe^+\}$ indicates that the two cations have similar ion-pair separation energies, for which the order might be dependent on the counterion.

One may notice that the ion-pair separation energies listed in Table 1 are those calculated for systems with R = Me. In real catalysts, R is usually represented by bulky alkyl groups. It is therefore necessary to explore the influence of the R groups on the ion-pair separation energy. To this end, calculations with R = CH_3 have been extended to R = H, ^{t}Bu (*tert*-butyl) as well. Due to the large size of the molecules, calculations have not been performed for all catalysts with the four different counterions listed in Table 1. Instead, only systems with $B(C_6F_5)_3Me^-$ as the counterion have been considered, except for $(Cp)(OSiR_3)TiMe^+$ where all four counterions were included. Table 2 displays the results for different sizes of R. It is obvious that increasing the size of R reduces the ion-pair separation energies significantly, especially when R is changed from Me to ^{t}Bu.

The size effect of the R groups may be, in the first place, due to the better electron-donating ability of ^{t}Bu compared to Me and especially H. Thus, an increase in the electron donation will enhance the stability of the metal center in the emerging cation species. In addition, the increasing size of the R groups is likely to destabilize the ion pair and lower the separation energy through steric interactions between R and the anion. We expect that at least half of the reduction in ΔH_{ips} is due to steric factors. Indeed, QM/MM calculations for the $(Cp)(OSi^tBu_3)TiMe{-}(\mu{-}Me){-}B(C_6F_5)_3$ system, in which the ^{t}Bu groups are represented by MM atoms, show that the ion-pair separation energy is 88.91 kcal/mol. The reduction in ΔH_{ips} from 94.96 kcal/mol for the full QM $(Cp)(OSiH_3)TiMe{-}(\mu\text{-}Me){-}B(C_6F_5)_3$ system to 88.91 kcal/mol for the QM/MM $(Cp)(OSi^tBu_3)TiMe{-}(\mu\text{-}Me){-}B(C_6F_5)_3$ system mainly comes from the steric effects of the ^{t}Bu groups, since the QM parts of the two systems are the same. We note that the reduction in ΔH_{ips} with increasing steric bulk is common for all four anions and that it increases to some degree with the number of R groups (Table 2).

Ion-Pair Formation Energy (Full QM). The ion-pair formation reaction is not the microscopic reverse process of ion-pair separation. Therefore, the ion-pair

Table 2. Full QM Ion-Pair Separation Energies (ΔH_{ips},[a] kcal/mol) for Different R Groups

		R		
counterion	catalyst	H	Me	^{t}Bu
$B(C_6F_5)_3Me^-$	$(NPR_3)_2TiMe^+$	82.43 (45.79)[b]	73.05 (41.59)	72.32 (42.46)
	$(Cp)(NPR_3)TiMe^+$	86.08 (50.71)	84.17 (50.86)	80.62 (49.00)
	$(Cp)(NCR_2)TiMe^+$	92.36 (55.78)	90.08 (54.87)	85.43 (51.04)
	$(CpSiMe_2NR)TiMe^+$	95.25 (58.31)	91.50 (56.52)	88.48 (53.16)
	$(Cp)(OSiR_3)TiMe^+$	94.96 (57.33)	91.49 (55.46)	83.26 (49.65)
$B(C_6F_5)_4^-$	$(Cp)(OSiR_3)TiMe^+$	80.83 (45.71)	76.84 (42.83)	66.53 (35.63)
TMAMAOMe$^-$	$(Cp)(OSiR_3)TiMe^+$	108.33 (68.57)	102.45 (64.18)	95.33 (59.42)
MAOMe$^-$	$(Cp)(OSiR_3)TiMe^+$	129.58 (85.50)	122.02 (79.20)	101.26 (60.87)

[a] Corresponding to the process $[LL'MMe]^+[A]^- \rightarrow [LL'MMe]^+ + A^- + \Delta H_{ips}$ where A = $MeB(C_6F_5)_3^-$, $B(C_6F_5)_4^-$, MAOMe$^-$, TMA-MAOMe$^-$. [b] In solution. Solvent: cyclohexane ($\epsilon = 2.023$).

Chart 1. Structures of Ion Pairs

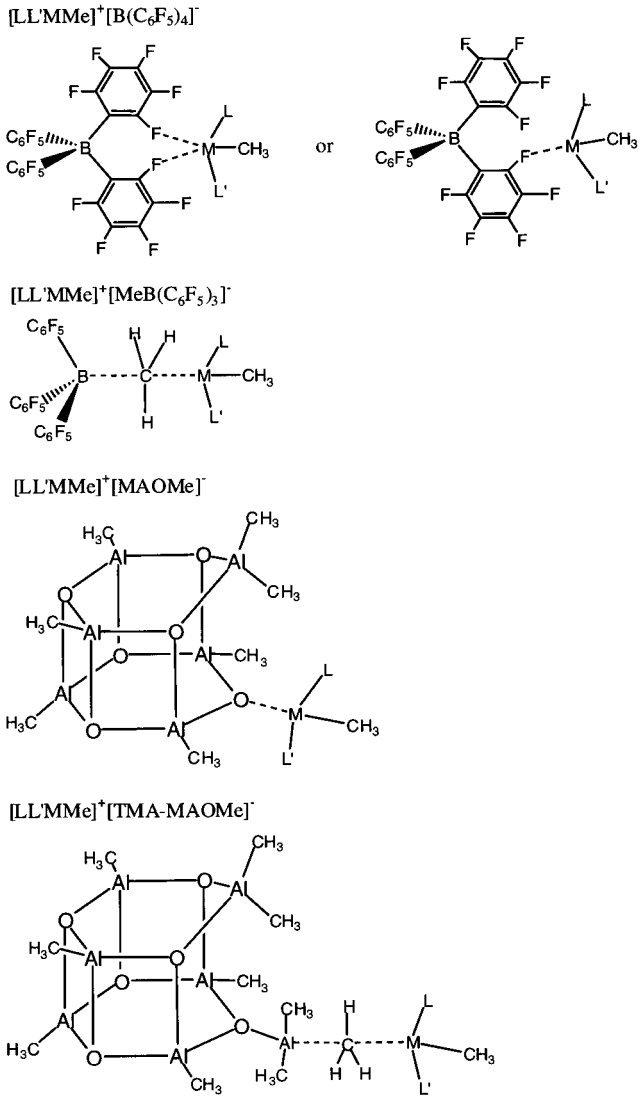

formation energy (ΔH_{ipf}) might not be a direct measure for the degree of mobility of the anion relative to the cation in the ion-pair. However, ΔH_{ipf} is an indication of the stability of the ion pair relative to the neutral constituents from which it is formed according to eq 1. Thus, ΔH_{ipf} must be below a certain threshold ($\Delta H_{ipf} <$ -10 to -15 kcal/mol) for the ion pair to exist on the free energy surface. We shall in the following examine if one can draw any correlation between the ion-pair formation and separation energies.

Table 3 displays the ion-pair formation energies calculated for systems with R = Me. Since the ion pairs of $B(C_6F_5)_4^-$ are not the direct products of the related precursors ($LL'MMe_2$) and the cocatalyst, their formation energies will not be discussed here. The ion pair containing $B(C_6F_5)_3Me^-$ is formed from a simple abstraction of a CH_3^- group by $B(C_6F_5)_3$ from $LL'MMe_2$ according to eq 1. The species $[LL'MMe]^+[MAOMe]^-$ is a product of a reaction in which an Al−O bond is broken in MAO followed by the migration of a methide group from $LL'MMe_2$ to aluminum in the broken Al−O linkage and the formation of a bond from the corresponding oxygen to the metal center (Ti or Zr) (Chart 1). The generation of $[LL'MMe]^+[TMA\text{-}MAOMe]^-$ follows the same route, except that a trimethylaluminum (TMA) molecule is inserted into the metal−oxygen bond (bottom of Scheme 1).

Among the titanium-based systems the ion-pair formation energy ΔH_{ipf} follows the trend

$$(NPMe_3)_2TiMe^+ < (Cp)(NPMe_3)TiMe^+ < (Cp)(NCMe_2)TiMe^+ < \{(CpSiMe_2NMe)TiMe^+, (Cp)(OSiMe_3)TiMe^+\} \quad (5)$$

for the three anions TMA-MAOMe$^-$, MAOMe$^-$, and $B(C_6F_5)_3Me^-$, which is exactly the same trend as for ΔH_{ips} in eq 4. Thus, the energy gained in forming the ion pair ($-\Delta H_{ipf}$) from its neutral constituents and the energy required to separate it into its ionic components follow exactly the opposite order with respect to the different titanium-based cations. Similar trends have also been found in previous studies (results shown in Table 4) on the formation of ion pairs involving $B(C_6F_5)_3Me^-$ and some group IV metallocenes.[23] The relationship existing between ΔH_{ips} and $-\Delta H_{ipf}$ for different cations reflects the fact that the cation in both processes acts as an acid that gives up a base in the form of either a methide group ($-\Delta H_{ipf}$) or the anion (ΔH_{ips}). Thus, with everything else equal within a series of cations and the same anion, the more acidic $[LL'MMe]^+$, the larger ΔH_{ips} and the smaller $-\Delta H_{ipf}$.

For the same cation and different anions, no correlation exists between $-\Delta H_{ipf}$ and ΔH_{ips}. This is understandable, since the ion-pair formation reaction is not the microscopic reverse process of ion-pair separation. Nevertheless, the most negative values of ΔH_{ipf} are calculated for the formation of the $[LL'MMe]^+[MAOMe]^-$ species, which also have the largest separation energies. This is again due to the strong M−O bond formed during the ion-pair formation. However, formation of

(23) Chan, M. S. W.; Vanka, K.; Pye, C. C.; Ziegler, T. *Organometallics* **1999**, *18*, 4624.

Table 3. Full QM Ion-Pair Formation Energies (ΔH_{ipf},[a] kcal/mol)

	$B(C_6F_5)_3$		TMA-MAO[b]		MAO	
precatalyst	gas phase	soln[c]	gas phase	soln[c]	gas phase	soln[c]
$(1,2\text{-}Me_2Cp)_2ZrMe_2$	−25.03	−24.97	−4.07	−4.46	−16.07	−14.86
$(NPMe_3)_2TiMe_2$	−27.77	−25.88	−15.29	−14.17	−29.92	−24.59
$(Cp)(NPMe_3)TiMe_2$	−26.55	−25.69	−13.55	−10.18	−29.39	−26.49
$(Cp)(NCMe_2)TiMe_2$	−24.56	−24.40	−11.96	−9.74	−30.52	−28.19
$(CpSiMe_2NMe)TiMe_2$	−14.58	−14.52	−5.47	−5.37	−25.99	−24.29
$(Cp)(OSiMe_3)TiMe_2$	−14.82	−12.78	−3.85	−1.51	−18.45	−14.77

[a] Corresponding to the process $LL'MMe_2 + A \rightarrow [LL'MMe]^+[MeA]^- + \Delta H_{ips}$, where $A = B(C_6F_5)_3$, MAO, TMA-MAO. [b] The most stable confirmation of TMA-MAO. See Chart 1. [c] Solvent: cyclohexane ($\epsilon = 2.023$).

Scheme 1. Formation of the Counterions MAOMe− and TMA-MAOMe−

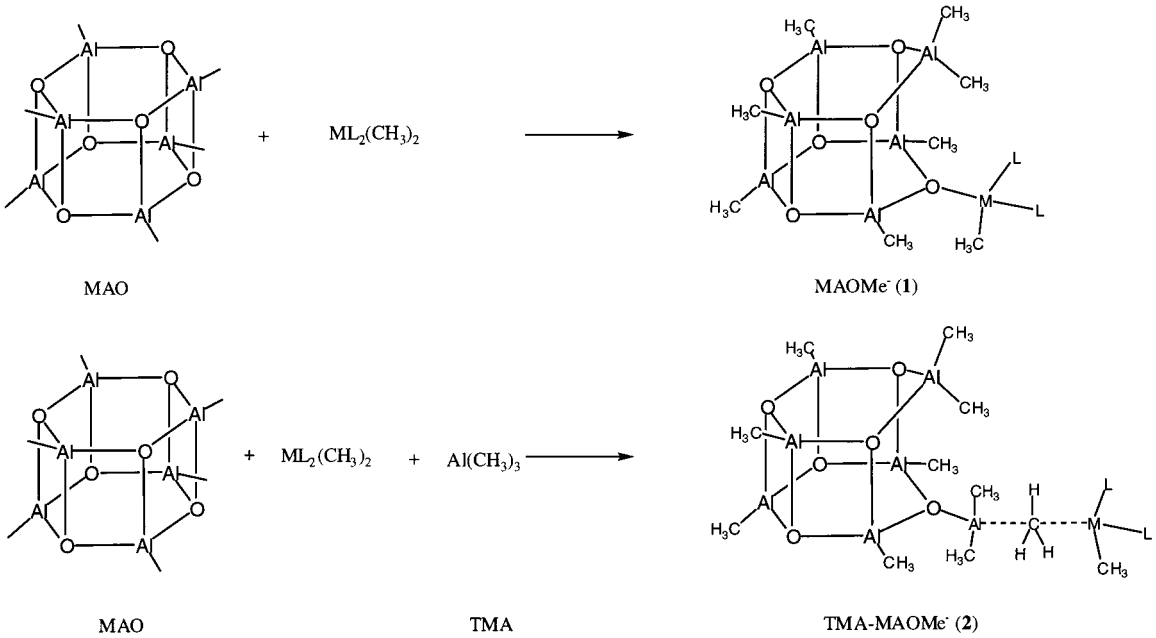

Table 4. Full QM Ion-Pair Formation and Separation Energies (kcal/mol) for Generic Model Catalysts (kcal/mol)

	ΔH_{ips}[a]		ΔH_{ipf}[b]	
catalyst	gas phase	soln[c]	gas phase	soln[c]
$(Cp)TiMe_2^+$	95.3	51.5	−12.9	−12.2
$(CpSiH_2NH)TiMe^+$	94.4	51.6	−13.9	−14.4
$(Cp)_2TiMe^+$	79.5	40.3	−15.5	−16.3
$(Cp)ZrMe_2^+$	95.8	49.7	−15.7	−14.9
$(CpSiH_2NR)ZrMe^+$	93.7	49.9	−16.6	−17.5
$(Cp)_2ZrMe^+$	88.5	48.5	−19.1	−19.1

[a] Corresponding to the process $LL'M(Me)-(\mu\text{-}Me)-B(C_6F_5)_3 \rightarrow (LL'MMe)^+ + (MeB(C_6F_5)_3)^- + \Delta H_{ips}$. [b] Corresponding to the process $LL'M(Me)_2 + B(C_6F_5)_3 \rightarrow LL'M(Me)-(\mu\text{-}Me)-B(C_6F_5)_3 + \Delta H_{ipf}$. [c] Solvent: toluene ($\epsilon = 2.38$).

$[LL'MMe]^+[B(C_6F_5)_3Me]^-$ is found to be more favorable than $[LL'MMe]^+[TMA\text{-}MAOMe]^-$, although the former is easier to separate.

Table 5 displays calculated ion-pair formation energies for different sizes of the R groups. On going from R = H to R = CH_3, one observes an increase in the exothermicity ($-\Delta H_{ipf}$) of the ion-pair formation process, as the better electron-donating ability of the methyl group makes the cation less acidic. In going next from R = CH_3 to R = ^{t}Bu one might have expected another increase in $-\Delta H_{ipf}$ on account of the better donor ability of ^{t}Bu. Instead, one observes only a marginal increase or decrease. This can be rationalized by the cancellation of the more favorable electronic factors by the larger steric demand of ^{t}Bu. It is worth recalling that the electronic and steric factors work in the same direction for the ion-pair separation process, where ΔH_{ips} is smallest for R = ^{t}Bu.

To understand the trends of the ion-pair formation and separation energies found above, attention has been given to the charge distributions and related structural features of the ion pairs studied. We mainly consider the charges of the ligands and the bond distances that are involved in the ion pair formations and separations.

The charges on the ligands L and L′ in $LL'TiMe_2$, q^P_k ($k = 1$ and 2, for L and L′, respectively), and $[LL'TiMe]^+$-$[MeB(C_6F_5)_3]^-$, q^I_k ($k = 1, 2$), were calculated by Hirshfeld analyses.[21] From these charges, one can calculate the donation of electrons from L or L′ as the ion pair is formed from the precursor as

$$\Delta q_k = q^I_k - q^P_k \tag{6}$$

The total number of donated electrons is given as

$$\Delta q_T = \Delta q_1 - \Delta q_2 \tag{7}$$

It follows from Table 6 that Δq_T correlates well with ΔH_{ips} and ΔH_{ipf} so that the strongest donating ligands (L and L′) give rise to the smallest values of ΔH_{ips} and ΔH_{ipf}.

We have also tried to correlate separation and formation energies to geometrical parameters of the ion pairs.

Table 5. Full QM Ion-Pair Formation Energies (ΔH_{ipf},[a] kcal/mol) for Different R Groups

		R		
counterion	catalyst	H	Me	^{t}Bu
$B(C_6F_5)_3Me^-$	$(NPR_3)_2TiMe^+$	−21.92 (−21.62)[b]	−27.73 (−25.88)	−29.37 (−29.20)
	$(Cp)(NPR_3)TiMe^+$	−20.26 (−21.07)	−26.55 (−25.69)	−26.94 (−26.87)
	$(Cp)(NCR_2)TiMe^+$	−17.64 (−18.14)	−24.56 (−24.40)	−19.79 (−19.36)
	$(CpSiMe_2NR)TiMe^+$	−13.92 (−14.44)	−14.58 (−14.52)	−15.92 (−16.01)
	$(Cp)(OSiR_3)TiMe^+$	−14.69 (−11.28)	−14.82 (−12.78)	−14.29 (−13.89)
TMA-$MAOMe^-$[c]	$(Cp)(OSiR_3)TiMe^+$	−6.13 (−2.53)	−3.85 (−1.51)	−4.43 (−3.67)
$MAOMe^-$	$(Cp)(OSiR_3)TiMe^+$	−22.41 (−17.70)	−18.45 (−14.77)	−5.39 (−3.36)

[a] Corresponding to the process $LL'MMe_2 + A \rightarrow [LL'MMe]^+[MeA]^- \Delta H_{ips}$ where $A = B(C_6F_5)_3$, MAO and TMA-MAO. [b] Solvent cyclohexane ($\epsilon = 2.023$). [c] The most stable confirmation of TMA-MAO. See Chart 1.

Table 6. Hirshfeld Charge Analysis for the Ti Systems with R = Me and $B(C_6F_5)_3Me^-$ as Anion

system	ligand (L or L′)	$q^P{}_k$[a]	$q^I{}_k$[b]	Δq_k[c]	Δq_T[d]
$(NPMe_3)_2TiMe^+$	$NPMe_3$	−0.0883	0.0170	0.1053	0.1909
	$NPMe_3$	−0.0945	−0.0089	0.0856	
$(Cp)(NPMe_3)TiMe^+$	$NPMe_3$	−0.0302	0.0761	0.1063	0.1783
	Cp	0.0062	0.0782	0.0720	
$(Cp)(NCMe_2)TiMe^+$	$NCMe_2$	−0.1207	−0.0784	0.0423	0.1729
	Cp	0.0404	0.1710	0.1306	
$(CpSiMe_2NMe)TiMe^+$	$CpSiMe_2NMe$	0.0149	0.1698	0.1549	0.1549
$(Cp)(OSiMe_3)TiMe^+$	$OSiMe_3$	−0.1828	−0.1135	0.0693	0.1448
	Cp	0.0633	0.1388	0.0755	

[a] Hirshfeld charge on L or L′ in $LL'TiMe_2$. [b] Hirshfeld charge on L or L′ in $LL'TiMe{-}(\mu\text{-}Me){-}B(C_6F_5)_3$ systems. [c] $\Delta q_k = q^I{}_k - q^P{}_k$ (k = 1, 2, for L and L′, respectively). [d] $\Delta q_T = \Delta q_1 + \Delta q_2$.

Table 7. Distances (Å) of Ti−C(μ-Me) and X−C(μ-Me) in Catalyst Systems with R = Me

	$B(C_6F_5)_3Me^-$		TMA-$MAOMe^-$	
catalyst	Ti−C(μ-Me)	B−C(μ-Me)	Ti−C(μ-Me)	Al−C(μ-Me)
$(NPMe_3)_2TiMe^+$	2.302	1.641	2.209	2.069
$(Cp)(NPMe_3)TiMe^+$	2.297	1.640	2.251	2.099
$(Cp)(NCMe_2)TiMe^+$	2.257	1.639	2.224	2.158
$(CpSiMe_2NMe)TiMe^+$	2.232	1.654	2.207	2.168
$(Cp)(OSiMe_3)TiMe^+$	2.206	1.662	2.143	2.252

The structural features of systems containing $B(C_6F_5)_4^-$ are complicated due to different coordination modes between Ti and $B(C_6F_5)_4^-$, and no clear correlation could be found. In the $MAOMe^-$ systems, besides the Ti−O bond, the additional Al−Ti interactions between the cation and anion makes it difficult as well to find correlations. For ion pairs with $B(C_6F_5)_3Me^-$ and TMA-$MAOMe^-$, the counterions interact with the cations through the well-defined μ-Me bridge. One expects that the ion-pair formation and separation energies may be closely related to the structural features of the μ-Me bridge. Table 7 shows the bond distances related to the μ-Me bridge. Indeed, the Ti−C(μ-Me) distances in the $MeB(C_6F_5)_3^-$ systems decrease as we descend Table 7, corresponding to an increase in the ion-pair separation energies shown in Table 1. For the TMA-$MAOMe^-$ system, the Al−C(μ-Me) distances increase as we descend Table 7, corresponding to a decrease in the formation energies shown in Table 3.

QM/MM Models for $B(C_6F_5)_3Me^-$ and TMA-$MAOMe^-$. The considerable size of the counterion makes full QM studies on monomer insertion in the presence of the counterion very expensive and time-consuming. Therefore, modeling of the counterion with QM/MM methods is an attractive alternative. As has been mentioned above, the interactions between cations and both $B(C_6F_5)_4^-$ and $MAOMe^-$ are quite complicated. Fortunately, $B(C_6F_5)_3Me^-$ and TMA-$MAOMe^-$ interact with the cations through a well-defined μ-Me bridge. We undertake here to develop QM/MM models for the counterions $B(C_6F_5)_3Me^-$ and TMA-$MAOMe^-$ and examined the models by looking at the interaction between the cation and anion in terms of ion-pair formation and separation energies.

For modeling of $B(C_6F_5)_3Me^-$ and TMA-$MAOMe^-$, the QM parts were represented by $MeBCl_3^-$ and $MeAlClMe_2^-$, respectively. The remaining atoms, i.e., the fluorinated phenyl groups and MAO atoms, were replaced by MM atoms (see Figure 5).

Ion-pair separation and formation energies were calculated using the QM/MM model for the counterions. The values of ΔH_{ips} and ΔH_{ipf} obtained were compared to the corresponding values for the full QM systems mentioned above. The comparison between the full QM and the QM/MM calculation results is shown in Table 8.

An inspection of the results shows that the values of ΔH_{ipf} for the QM/MM systems are in close agreement with the corresponding estimates for the full QM system. This suggests that the process of abstracting the methide group from the precatalyst to form the contact ion pair is successfully modeled by the QM/MM system. However, the value of ΔH_{ips} for the QM/MM systems, in comparison to their QM counterparts, are higher by about 10−17 kcal/mol for all the cases studied. This means that the energy required to separate the ions in the ion pair to infinite distance is overestimated by 10−17 kcal/mol by the QM/MM model in the gas phase. The error is reduced to about 3−8 kcal/mol (data in parentheses in Table 8) in the solvent phase. However, it should be mentioned here that total separation of the anion from the cation is a process that is unlikely to occur during the insertion of the monomer into the metal−alkyl bond. Calculations have suggested that, for systems with the counterion $MeB(C_6F_5)_3^-$, the anion is only slightly displaced from the cation (about 1−1.5 Å)

Table 8. Comparison of Separation and Formation Energies (kcal/mol) Calculated Using QM and QM/MM Methods

		ΔH_{ips}		ΔH_{ipf}	
counterion	catalyst	QM	QM/MM	QM	QM/MM
$B(C_6F_5)_3Me^-$	$(NPH_3)_2TiMe^+$	81.8 (45.8)[a]	93.6 (48.9)	−22.3	−21.0
	$(Cp)(NCMe_2)TiMe^+$	87.4 (52.4)	97.6 (55.6)	−24.1	−21.9
	$(Cp)_2TiMe^+$	79.5 (47.1)	94.1 (52.1)	−15.5	−15.4
	$(Cp)TiMe_2+$	95.3 (58.2)	107.8 (62.8)	−12.9	−11.0
	$(CpSiH_2NH)TiMe^+$	94.4 (54.6)	105.0 (61.0)	−13.9	−11.2
	$(CpSiMe_2NH)TiMe^+$	90.4 (55.4)	102.6 (61.7)	−13.3	−15.1
	$(Cp)(OSiH_3)TiMe^+$	93.6 (56.3)	105.3 (61.9)	−10.4	−10.2
	$(1,2Me_2Cp)_2ZrMe^+$	80.5 (49.6)	95.6 (54.1)	−22.8	−24.8
	$(Cp)_2ZrMe^+$	88.5 (50.2)	99.5 (56.8)	−19.1	−18.7
	$(Cp)ZrMe_2+$	93.3 (51.6)	103.3 (59.7)	−15.7	−13.3
	$(CpSiH_2NH)ZiMe^+$	92.4 (51.8)	106.2 (58.4)	−16.6	−13.1
TMA-MAOMe$^-$	$(NPH_3)_2TiMe^+$	91.4	108.4	−9.8	−15.4
	$(Cp)(NCMe_2)TiMe^+$	99.4	110.5	−12.0	−14.2
	$(CpSiMe_2NMe)TiMe^+$	104.3	117.9	−5.5	−9.4
	$(Cp)(OSiH_3)TiMe^+$	108.3	123.8	−6.1	−8.2

[a] Including solvation effect. Solvent: toluene ($\epsilon = 2.38$).

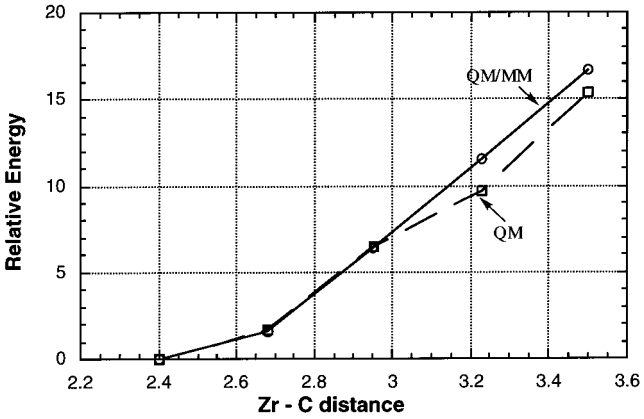

Figure 6. Comparison between QM and QM/MM energy profiles of Zr−μ-C bond displacement for the (1,2-Me_2-Cp)$_2$ZrMe−(μ-Me)−$B(C_6F_5)_3$ ion-pair system.

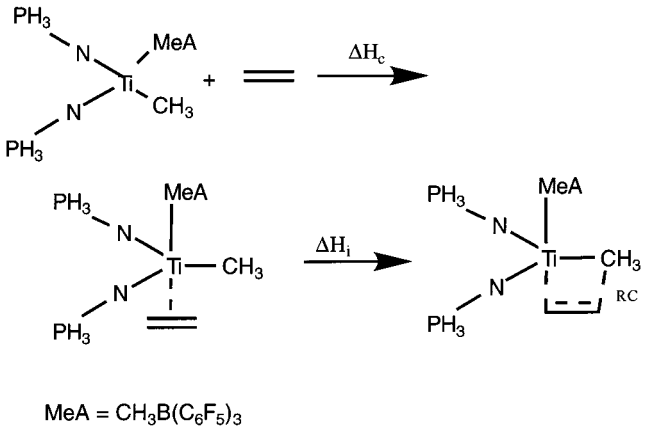

ΔH_c Full QM Calculation : **+1.51 kcal/mol**; QM/MM Calculation : **-0.73 kcal/mol**

ΔH_i Full QM Calculation : **+5.90 kcal/mol**; QM/MM Calculation : **+4.00 kcal/mol**

Figure 7. Uptake and insertion of the ethylene monomer into $(NPH_3)_2TiMe-(\mu\text{-}Me)-B(C_6F_5)_3$.

when insertion occurs, i.e., the "insertion region" for the ion pair corresponds to a displacement of about 1−1.5 Å of the anion. It is, therefore, the behavior of the QM/MM model in this insertion region that should be of primary interest. With this in mind, a comparative study between the full QM system and the QM/MM model was carried in the insertion region with the (1,2-Me_2Cp)$_2$ZrMe−(μ-Me)−$B(C_6F_5)_3$ ion-pair system. The Zr−μ-C distance was varied from 2.4 Å— which is the value in the QM optimized ion pair—to about 3.5 Å, for both the QM and QM/MM models. The increase in energy of the ion-pair system with the increase in the Zr−μ-C distance was plotted in Figure 6. The energy of the optimized ion pair was taken as the reference—"0" value in both the QM and the QM/MM cases. From this figure, it is clear that the change in energy is similar for both cases, implying that the QM/MM model is likely to behave similarly to the QM system in the "insertion region". Since this is the principal region of interest in polymerization studies, the QM/MM model for the $B(C_6F_5)Me^-$ counterion is deemed to be satisfactory.

A further validation of the model for $B(C_6F_5)Me^-$ was done by conducting a comparison of an insertion of a monomer ethylene into the metal−alkyl bond. Full QM and QM/MM calculations were carried out for the $(NPH_3)_2TiMe-(\mu\text{-}Me)-B(C_6F_5)_3$ catalyst system. The insertion process involved the uptake of the ethylene monomer to form the $C_2H_4-(NPH_3)_2TiMe-(\mu\text{-}Me)-B(C_6F_5)_3$ π complex and the subsequent internal barrier leading to the formation of the transition state prior to insertion. The processes of uptake and insertion are illustrated in Figure 7, along with the values of ΔH_c and ΔH_i obtained from the QM and QM/MM calculations on the $(NPH_3)_2TiMe-(\mu\text{-}Me)-B(C_6F_5)_3$ systems. With the QM/MM model, the differences in the values of ΔH_c and ΔH_i are relatively minor: i.e., in the acceptable range of 1.5−2.0 kcal/mol. In the $C_2H_4-(NPH_3)_2TiMe-(\mu\text{-}Me)-B(C_6F_5)_3$ π complex, the distance between the carbons of the ethylene and the titanium are about 2.6 Å for both the QM and the QM/MM systems. The principal geometry features in the transition-state geometries are also similar in both cases—the Ti−ethylene carbon distances (2.4 Å) and the distance between the α-carbon on the ethylene and the carbon on the methyl group attached to titanium (2.3 Å), which was considered as the reaction coordinate (RC). Overall, the results suggest that the QM/MM model for

$B(C_6F_5)_3Me^-$ satisfactorily reproduces the behavior of the ion-pair system in the insertion region. It should be pointed out here that only one possible reaction path has been explored.

A preliminary study on the insertion of ethylene into the metal−alkyl bond of $(NPH_3)_2TiMe-(\mu\text{-}Me)-$TMA-MAO shows that the insertion barriers (ΔH_i) calculated using full QM and QM/MM methods are ∼20 kcal/mol and ∼18 kcal/mol, respectively. The difference is about 2 kcal/mol, also in the acceptable range. Our initial calculations suggest that the QM/MM model for TMA-MAO should also be a good model for further study of the insertion reaction mechanisms.

It should be pointed out here that only one possible reaction path for both systems mentioned above has been explored. The insertion barriers obtained may not relate to the real activity of the catalysts, since other possible reaction paths have not been investigated. Nevertheless, our purpose here is to verify our QM/MM models by looking at the same reaction path and comparing the QM/MM results with the full QM results.

Conclusion

We have so far studied the interactions between series of cationic catalysts and anionic counterions in terms of ion-pair formation and separation energies using both full QM and hybridized QM/MM methods. In summary, the calculation results give the following conclusions.

(1) Among the four counterions $B(C_6F_5)_4^-$, $MeB(C_6F_5)_3^-$, TMA-$MAOMe^-$, and $MAOMe^-$ studied here, $B(C_6F_5)_4^-$ has the lowest ion-pair separation energy with the cations, indicating the weakest interactions between $B(C_6F_5)_4^-$ and the cations. For the same catalyst system, the ion-pair separation energy increases in the sequence $B(C_6F_5)_4^- < MeB(C_6F_5)_3^- <$ TMA-$MAOMe^- < MAOMe^-$. Here, two simplified model structures, which have been proposed as the counterions for the active (TMA-$MAOMe^-$) and dormant ($MAOMe^-$) ion pairs in single-site catalysts activated by MAO, were used for the last two counterions.

(2) For the same counterion and R = Me, the $(NPR_3)_2TiMe^+$ systems have the lowest separation energy, even lower than that of $(1,2\text{-}Me_2Cp)_2ZrMe^+$. The separation energies for the $(Cp)(NPR_3)TiMe^+$ systems are calculated to be about 10 kcal/mol higher than for $(NPR_3)_2TiMe^+$. The other three systems, $(Cp)(NCR_2)TiMe^+$, $(CpSiR_2NMe)TiMe^+$, and $(Cp)(OSiR_3)TiMe^+$, have similar separation energies, about 10 kcal/mol higher than those of $(Cp)(NPMe_3)TiMe^+$. Increasing the size of the R groups decreases the ion-pair separation energy for all systems studied due to both electronic and steric factors.

(3) The ion-pair formation energies for the Ti catalysts with R = Me and the same counterion are found to be related to the ion-pair separation energies: i.e., a lower separation energy corresponds to a more negative ion-pair formation energy. For systems with different counterions, no relationship between separation and formation energy has been found. Increasing the size of the R group has only a modest influence on the ion-pair formation energy, due to a cancellation of steric (destabilizing) and electronic (stabilizing) effects.

(4) QM/MM models for $B(C_6F_5)_3Me^-$ and TMA-$MAOMe^-$ have been developed and examined by comparing the ion-pair formation and separation energies to the full QM results. The QM parts of $B(C_6F_5)_3Me^-$ and TMA-$MAOMe^-$ are represented by $MeBCl_3^-$ and $MeAlClMe_2$, respectively. The other parts of the anions are replaced by MM atoms. Preliminary studies on olefin insertion reactions for the $(NPH_3)_2TiMe-(\mu\text{-}Me)-$A systems suggest that the QM/MM models satisfactorily reproduce the behavior of the ion-pair system in the insertion.

Acknowledgment. This investigation was supported by the Natural Science and Engineering Research Council of Canada (NSERC) and by Nova Research and Technology Corp. (NRTC) of Calgary.

Supporting Information Available: Tables giving Cartesian coordinates for full QM optimized ion-pair geometries. This material is available free of charge via the Internet at http://pubs.acs.org.

OM011057C